ISSN: 1001-4055 Vol. 44 No.6 (2023)

Peristaltic Transport of (Al₂O₃/H₂O) Nanofluid through A Vertical Asymmetric Channel with MHD Effects

P Praveen Kumar 1,2,*, S Balakrishnan 1 and A Magesh 3

¹Department of Mathematics, Islamiah College, Vaniyambadi, India 635 752.

²Department of Mathematics, Sathya College of Arts and Science, Kilvisharam, India 632 509.

³Department of Mathematics, Sri Sai Ram Engineering College, Chennai, India 600 044.

Abstract: In this investigation, we analyzed the effect of the magnetic field on the peristaltic motion of the (Al_2O_3/H_2O) nanofluid in a vertical asymmetrical channel utilizing heat and mass transfer. The present problem's unsteady governing equations are modulated. After converting the unstable equations into steady equations and applying the lubrication theory approximation, the long equations are reduced. The perturbation method is used to solve coupled nonlinear differential equations analytically (such as the concentration and temperature equations). The stream function's exact solution is also computed. Plotting the velocity profile, pressure rise, temperature, and concentration data is done using MATLAB, while generating the streamlines is performed with MATHEMATICA.

Keywords: Nanofluid, Heat and Mass transfer, Peristaltic transport, MHD

1. Introduction

Peristalsis refers to the gradual wave of surface contraction and expansion on the pliable wall of a conduit or channel that transfers fluid from a low-pressure to a high-pressure region. By selecting the peristaltic wave train that passes through the walls with different phase angles and wave amplitudes, an asymmetric channel is created. Recently, scientists have become intrigued by their extensive utility in the fields of manufacturing, physiology, and engineering. This principle is utilized in numerous glandular ducts and physiological processes, including the movement of urine from the kidney to the bladder, the rhythmic motion of the digestive system, the flow of intrauterine fluid, the vasomotion of the small blood vessels, and the lymph in the lymph vessels. There are several industrial uses for this system, including the transportation of caustic liquids in the nuclear sector, hazardous liquids, sanitary liquids, sensitive materials, etc. Some attempts dealing with peristalsis are presented in [1-4].

Magnetohydrodynamic (MHD) physiological fluid peristaltic movement is significant in medicine and bioengineering. In fact, the motion of a conducting liquid across a magnetic field induces an electric current. When a magnetic field acts on a current, mechanical forces emerge that alter the fluid's path. The principles of MHD are used in the functioning of compressors, blood pump machines, heat exchanger design, flow meter design, power generator design, radar system design, and many more applications. These types of bioengineering and medical science principles have been used for a wide variety of applications, including the transport of targeted medications, the reduction of surgical bleeding, the creation of magnetic devices for cell separation, the creation of magnetic tracers, hyperthermia, and many others. Magnetic field therapy typically makes use of MHD non-Newtonian materials. In particular, MHD peristaltic flows are important for solving problems with the urinary system, altering the behaviour of cells and tissues, and treating conditions associated

with gastrointestinal motility. In light of these considerations, there have been various developments for peristaltic flows of MHD fluids in a channel [5-8].

The term "nanofluid" refers to a conventional fluid (water, Ethelyn glycol, oil, etc.,) that contains nanoparticles (TiO₂,Al₂O₃,SiO₂,etc.,) and possesses considerable practical utility across various domains, including but not limited to size exclusion chromatography, neuroelectronic interfaces, in vivo therapy, protein engineering, cancer diagnostics and therapy, and nonporous materials. Scientists, engineers, and physiologists are presently very interested in the study of nanofluids that are associated with peristaltic activity due to these applications. Some researchers in the scientific community are of the opinion that the utilization of nanofluids can help control overeating. A few current studies on nanofluid activity under various assumptions may be seen in the attempts [9-14].

The objective of the current experiment is to investigate the influence that magnetohydrodynamic flow of heat and mass transfer has on the peristaltic transport of alumina water (Al_2O_3/H_2O) nanofluid along an asymmetric vertical channel. After the appropriate governing equations have been created, the length equations can be simplified by taking into account of large wavelength $(\lambda \to \infty)$ and the low Reynolds number $(Re \to 0)$ assumptions. By employing the series solution obtained through the perturbation approach, analytical methods are utilized to determine the solutions to the resulting two-dimensional coupled nonlinear differential equations. The graphical representations of the frequency distribution, velocity profile, and nanoparticle volume fraction for the alumina water nanofluid were generated utilizing the Matlab software. In addition, the contour plots for the stream function are illustrated using the Mathematica software. In conclusion, a detailed explanation of the most significant things that can be learned from the findings. This work can be extended with Hybrid nanofluids.

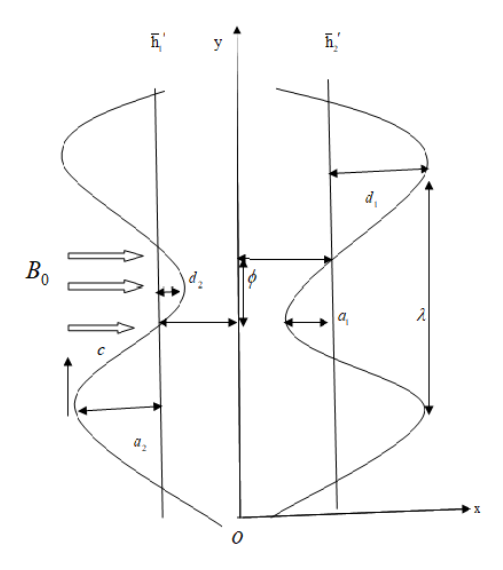


Figure 1. Flow Geometry

2. Mathematical formulation

Peristaltic motion of two-dimensional viscous, incompressible (Al_2O_3/H_2O) nanofluid via an asymmetric vertical channel walls covered by h'_1 and h'_2 see Figure 1. The flow is propagated by sinusoidal wave trains with constant wave speed c in the direction of \widetilde{X}' are given by

$$h_1'\!\left(\tilde{X}',\tilde{t}'\right)\!=\!-d_2^{}-a_2^{}\cos\frac{2\pi}{\lambda}\!\left(\tilde{X}'\!-\!c\tilde{t}'\right)\!+\!\varphi$$

$$h_2'\left(\tilde{X}',\tilde{t}'\right) = d_1 + a_1 \cos\frac{2\pi}{\lambda} \left(\tilde{X}' - c\tilde{t}'\right) \tag{1}$$

Here wave speed c, channel width d_1+d_2 , the wave amplitudes a_2,a_1 , phase difference $\phi\in[0,\pi]$, $\phi=0$ then the waves are out phase (symmetric channel) and $\phi=\pi$ then the waves are in phase. Moreover, d_2,d_1,a_2,a_1 , ϕ satisfies the relation

$$a_1^2 + a_2^2 + 2a_1a_2\cos\phi \le (d_2 + d_1)^2$$
 (2)

The nanofluids thermophysical properties are

$$(\rho c_{p})_{nf} = \tilde{\varpi}'(\rho c_{p})_{s} + (1 - \tilde{\varpi}')(\rho c_{p})_{f}, \ \sigma_{nf} = \frac{3\tilde{\varpi}'(\sigma_{s} - \sigma_{f})}{\left(\frac{\sigma_{s}}{\sigma_{f}} + 21\right) + \left(1 - \sigma_{f}\sigma_{s}\right)} + \sigma_{f}, \ \rho_{nf} = (1 - \tilde{\varpi}')\rho_{f} + \tilde{\varpi}'\rho_{s},$$

here $\tilde{\varpi}'$ is the nanofluids solid fractional volume, σ_{nf} , $(\rho c_p)_{nf}$ and ρ_{nf} are the nanofluids electrical conductivity, specific heat and density.

The governing equations are

$$\begin{split} \rho_{nf} \Bigg[\frac{\partial \overline{U}}{\partial \overline{t}} + \overline{U} \frac{\partial \overline{U}}{\partial \overline{X}} + \overline{V} \frac{\partial \overline{U}}{\partial \overline{Y}} \Bigg] &= \frac{\partial \overline{P}}{\partial \overline{X}} + \frac{\partial S_{XX}}{\partial \overline{X}} + \frac{\partial S_{XY}}{\partial \overline{Y}} - \frac{\sigma_{nf} B_0^2 \overline{U}}{\mu_{nf}} \\ &\quad + \left(1 - C_0 \right) \rho_{nf} g_\alpha \left(T - T_0 \right) + \left(\rho_p - \rho_{nf} \right) g_\beta \left(C - C_0 \right) (3) \\ \rho_{nf} \Bigg[\frac{\partial \overline{V}}{\partial \overline{t}} + \overline{U} \frac{\partial \overline{V}}{\partial \overline{X}} + \overline{V} \frac{\partial \overline{V}}{\partial \overline{Y}} \Bigg] &= \frac{\partial \overline{P}}{\partial \overline{Y}} + \frac{\partial S_{XY}}{\partial \overline{X}} + \frac{\partial S_{YY}}{\partial \overline{Y}} \\ \left(\rho C_p \right)_{nf} \Bigg[\frac{\partial \overline{U}}{\partial \overline{t}} + \overline{U} \frac{\partial \overline{U}}{\partial \overline{X}} + \overline{V} \frac{\partial \overline{U}}{\partial \overline{Y}} \Bigg] &= K_{nf} \left(\frac{\partial^2 T}{\partial \overline{X}^2} + \frac{\partial^2 T}{\partial \overline{Y}^2} \right) \\ &\quad + \left(\rho C_p \right)_{nf} D_B \Bigg[\frac{\partial \overline{C}}{\partial \overline{X}} \frac{\partial \overline{U}}{\partial \overline{X}} + \frac{\partial \overline{C}}{\partial \overline{Y}} \frac{\partial \overline{U}}{\partial \overline{Y}} \Bigg] + \frac{D_T}{T_M} \left(\rho C_p \right)_{nf} \Bigg[\left(\frac{\partial T}{\partial X} \right)^2 + \left(\frac{\partial T}{\partial Y} \right)^2 \right] (5) \\ \Bigg[\frac{\partial \overline{C}}{\partial \overline{t}} + \overline{U} \frac{\partial \overline{C}}{\partial \overline{X}} + \overline{V} \frac{\partial \overline{C}}{\partial \overline{Y}} \Bigg] &= D_B \Bigg[\frac{\partial^2 C}{\partial \overline{X}^2} + \frac{\partial^2 C}{\partial \overline{Y}^2} \Bigg] + \frac{D_T}{T_M} \Bigg[\frac{\partial^2 T}{\partial \overline{X}^2} + \frac{\partial^2 T}{\partial \overline{Y}^2} \Bigg] \end{aligned} \tag{6}$$

In which \tilde{V}', \tilde{U}' are the velocities in \tilde{Y}', \tilde{X}' directions, \tilde{P}' , \tilde{t}' , B_0 , \tilde{C}' , \tilde{T}' , T_M , k_1 , D_T , and D_B are the pressure, time, electrically conducting magnetic field, concentration, temperature, mean temperature, chemical reaction parameter, thermophoresis parameter and Brownian diffusion coefficient respectively.

Physical properties	$\rho(\text{kgm}^{-3})$	$c_p(Jkg^{-1}K^{-1})$	k(Wm ⁻¹ K ⁻¹)	$\mu(Kgm^{-1}s^{-1})$	$\sigma(Sm^{-1})$
Water (H ₂ O)	997.0	4179.0	0.613	8.91×10^{-4}	0.05
Al_2O_3	3970.0	765.0	38.5	-	-

Table 1.Thermophysical properties of water and Al₂O₃

The (Al₂O₃ / H₂O) nanofluids thermal conductivity, Prandtl number and viscosity (Table 1) are described as

$$k_{nf} = (4.97\tilde{\varpi}'^2 + 2.72\tilde{\varpi}' + 1)k_f, Pr_{nf} = (82.1\tilde{\varpi}'^2 + 3.9\tilde{\varpi}' + 1)Pr_f, s \ \mu_{nf} = (123\tilde{\varpi}'^2 + 7.3\tilde{\varpi}' + 1)\mu_f, (7)$$

Introducing Galilean Transformation

$$\overline{y} = \overline{Y}, \overline{u} = \overline{U} - C, \overline{x} = \overline{X} - c\overline{t}, \overline{v} = \overline{V}$$
 (8)

Applying Eq.(8) into Eqs. (3)-(6) we get

$$\frac{\partial \overline{\mathbf{u}}}{\partial \mathbf{x}} + \frac{\partial \overline{\mathbf{v}}}{\partial \overline{\mathbf{y}}} = 0 \tag{9}$$

$$\rho_{nf} \left[-C \frac{\partial \overline{u}}{\partial \overline{x}} + (\overline{u} + C) \frac{\partial \overline{u}}{\partial \overline{x}} + \overline{v} \frac{\partial \overline{u}}{\partial \overline{y}} \right] = -\frac{\partial \overline{p}}{\partial \overline{x}} + \frac{\partial S_{xx}}{\partial \overline{x}} + \frac{\partial S_{xy}}{\partial \overline{y}} - \frac{\sigma_{nf}}{\sigma_{f}} (u + 1) + (1 - C_{0}) \rho_{nf} g_{\alpha} (T - T_{0}) + (\rho_{p} - \rho_{nf}) g_{\beta} (C - C_{0})$$
(10)

$$\rho_{\rm nf} \left[-C \frac{\partial \overline{v}}{\partial \overline{x}} + \left(\overline{u} + C \right) \frac{\partial \overline{u}}{\partial \overline{x}} + \overline{v} \frac{\partial \overline{u}}{\partial \overline{y}} \right] = -\frac{\partial \overline{p}}{\partial \overline{y}} + \frac{\partial S_{xy}}{\partial \overline{x}} + \frac{\partial S_{yy}}{\partial \overline{y}}$$

$$\tag{11}$$

$$\begin{split} \left(\rho C_{_{p}}\right)_{_{nf}} & \left[-C \frac{\partial \overline{T}}{\partial \overline{x}} + \left(\overline{u} + C\right) \frac{\partial \overline{T}}{\partial \overline{x}} + \overline{v} \frac{\partial \overline{T}}{\partial \overline{y}} \right] = K_{_{nf}} \left(\frac{\partial^{2} T}{\partial \overline{x}^{2}} + \frac{\partial^{2} T}{\partial \overline{y}^{2}} \right) \\ & + \left(\rho C_{_{p}}\right)_{_{nf}} D_{_{B}} \left[\frac{\partial \overline{C}}{\partial \overline{x}} \frac{\partial \overline{T}}{\partial \overline{x}} + \frac{\partial \overline{C}}{\partial \overline{y}} \frac{\partial \overline{T}}{\partial \overline{y}} \right] + \frac{D_{_{T}}}{T_{_{M}}} \left(\rho C_{_{p}}\right)_{_{nf}} \left[\left(\frac{\partial T}{\partial \overline{x}} \right)^{2} + \left(\frac{\partial T}{\partial \overline{y}} \right)^{2} \right] \end{split}$$

$$\left[-C \frac{\partial \overline{C}}{\partial \overline{x}} + \left(\overline{u} + C \right) \frac{\partial \overline{C}}{\partial \overline{x}} + \overline{v} \frac{\partial \overline{C}}{\partial \overline{y}} \right] = D_{\mathbf{B}} \left[\frac{\partial^{2} C}{\partial \overline{x}^{2}} + \frac{\partial^{2} C}{\partial \overline{y}^{2}} \right] + \frac{D_{\mathbf{T}}}{T_{\mathbf{M}}} \left[\frac{\partial^{2} T}{\partial \overline{x}^{2}} + \frac{\partial^{2} T}{\partial \overline{y}^{2}} \right]$$
(13)

The dimensionless variables are

$$\begin{split} x &= \frac{\overline{x}}{\lambda}, y = \frac{\overline{y}}{d_{_{1}}}, h_{_{1}} = \frac{\overline{h}_{_{1}}}{d_{_{1}}}, h_{_{2}} = \frac{\overline{h}_{_{2}}}{d_{_{1}}}, \delta = \frac{d_{_{1}}}{\lambda}, P = \frac{d_{_{1}}^{2}\overline{p}}{c\mu_{_{f}}\lambda}, u = \frac{\overline{u}}{c}, v = \frac{\overline{v}}{c\delta}, Pr_{_{nf}} = \frac{\mu_{_{f}}\left(C_{_{p}}\right)_{_{f}}}{k_{_{f}}}, Re = \frac{\rho_{_{f}}cd_{_{1}}}{\mu_{_{f}}} \\ \phi &= \frac{\overline{C} - C_{_{0}}}{C_{_{1}} - C_{_{0}}}, \theta = \frac{\overline{T} - T_{_{0}}}{T_{_{1}} - T_{_{0}}}, G_{_{T}} = \frac{\left(1 - C_{_{0}}\right)\rho_{_{f}}g_{_{\alpha}}d_{_{1}}^{2}\left(T_{_{1}} - T_{_{0}}\right)}{C\mu_{_{f}}}, G_{_{n}} = \frac{\left(\rho_{_{p}} - \rho_{_{f}}\right)g_{_{\beta}}d_{_{1}}^{2}\left(C_{_{1}} - C_{_{0}}\right)}{C\mu_{_{f}}}, M = \sqrt{\frac{\sigma_{_{f}}}{\mu}}B_{_{0}}d_{_{1}}, \\ N_{_{b}} &= \frac{\tau D_{_{B}}\rho_{_{f}}\left(C_{_{1}} - C_{_{0}}\right)}{\mu_{_{f}}}, N_{_{t}} = \frac{\tau D_{_{T}}\rho_{_{f}}\left(T_{_{1}} - T_{_{0}}\right)}{T_{_{M}}\mu_{_{f}}}, \tau = \frac{\left(\rho C_{_{p}}\right)_{_{nf}}}{\left(\rho C_{_{p}}\right)_{_{f}}}, S_{_{XX}} = \frac{\lambda}{C\mu_{_{f}}}S_{_{X\bar{X}}}, S_{_{XY}} = \frac{d_{_{1}}}{C\mu_{_{f}}}S_{_{XY}}, S_{_{YY}} = \frac{d_{_{1}}}{C\mu_{_{f}}}S_{_{YY}} \\ \end{array}$$

where Nb, Pr_f , Nt, γ , Re and τ are Brownian motion parameter, Prandtl number, thermophoresis diffusion parameter, chemical reaction parameter, Reynold's number and effective heat capacity.

The stream functions is

$$u = \frac{\partial \psi}{\partial y}$$
 and $v = -\frac{\partial \psi}{\partial x}$

Applying Eq.(14) into Eqs.(10)-(14), and assumptions of low Reynolds number, long wavelength approximations, and into Eqs.(10)-(14) in terms of stream function as follows

$$\frac{\partial P}{\partial x} = -\frac{\partial S_{xy}}{\partial y} + \frac{\rho_{nf}}{\rho_{f}} G_{T} \theta + G_{n} \phi - \frac{\sigma_{nf}}{\sigma_{f}} M^{2} (\psi_{y} + 1) (15)$$

Vol. 44 No.6 (2023)

$$\frac{\partial P}{\partial v} = 0 (16)$$

$$\frac{\partial^{2} \theta}{\partial y^{2}} + \Pr Nb \frac{k_{f}}{k_{nf}} \frac{\partial \varphi}{\partial y} \frac{\partial \theta}{\partial y} + \Pr Nt \frac{k_{f}}{k_{nf}} \left(\frac{\partial \theta}{\partial y} \right)^{2} = 0$$
(17)

$$\frac{\partial^2 \varphi}{\partial y^2} + \frac{Nt}{Nb} \frac{\partial^2 \theta}{\partial y^2} = 0 \ (18)$$

where

$$S_{xy} = -\frac{\mu_{nf}}{\mu_{f}} \left(\frac{\partial^{2} \psi}{\partial y^{2}} \right), \tag{19}$$

From Eqs.(15) and (16)

$$0 = -\frac{\mu_{\rm nf}}{\mu_{\rm f}} \left(\frac{\partial^4 \psi}{\partial y^4} \right) + \frac{\rho_{\rm nf}}{\rho_{\rm f}} G_{\rm T} \frac{\partial \theta}{\partial y} + G_{\rm n} \frac{\partial \phi}{\partial y} - \frac{\sigma_{\rm nf}}{\rho_{\rm f}} M^2 \left(\frac{\partial^2 \psi}{\partial y^2} \right)_{(20)}$$

The boundary conditions are

$$\psi = -\frac{F}{2}, \ \psi_{y} = -1, \ \theta = 0, \phi = 0 \text{ at } y = h_{1} = -d - b\cos(x + \phi),$$
(21)

$$\psi = \frac{F}{2}$$
, $\psi_y = -1$, $\theta = 1$, $\phi = 1$ at $y = h_2 = 1 + a \cos x$,

3. Solution of the Methodology

Eqs.(17) and (18) are coupled nonlinear partial differential equations. It is therefore impossible to calculate an exact solution. Consequently, the regular perturbation method is used to derive serial solutions for the small parameter \tilde{p}' . Thus, we develop θ and φ as follows

$$\theta = \theta_0 + \tilde{\mathbf{p}}'\theta_1 + \tilde{\mathbf{p}}'^2\theta_2 + \dots \tag{22}$$

$$\varphi = \varphi_0 + \tilde{p}'\varphi_1 + \tilde{p}'^2\varphi_2 + ... (23)$$

Substitute the result of Eqs (17) and (18) into Eqs.(22), (23) and $\overline{p}' \rightarrow 1$ we get directly as follows

$$\theta = c_1 y + c_2 + c_3 y + c_4 + \frac{y^2}{2} A_2 \tag{24}$$

$$\varphi = c_1 y + c_2 + c_5 y + c_6 - \frac{N_t}{N_b} A_2 \frac{y^2}{2}$$
(25)

Exact solution of Eq. (20) with the help of Eq. (21) is as follows

$$\psi = B_1 + B_2 y + B_3 y^2 + B_4 y^3 + A_9 e^{-A_2 y} + A_{10} y^4$$
(26)

Due to page restrictions, all the constants appeared in Eqs (24)-(26) are ignored. The pressure rise Δp_{λ} for single wavelength is defined by

-____

$$\Delta p_{\lambda} = \int_{0}^{2\pi} \frac{dp}{dx} dx \ (27)$$

4. Result and Discussion

4.1. Velocity and pressure rise

This section presents the graphical analysis of the fluid velocity, Pressure rise, temperature, concentration and stream functions for a variety of significant parameter values. The variation of the velocity profile for the Hartmann number was shown in Figure 2(a). This graphic shows that the (Al_2O_3/H_2O) nanofluid's velocity decreased for Magneto hydrodynamic flow near the centre of the channel. The fact underlying this action is the resistive nature of Lorentz force, which reduces fluid velocity. Therefore, the bigger magnetic number's opposite behaviour is advantageous for treating conditions like depression, cancer, joint difficulties, and migraine headaches. Impact of ϕ on velocity profile is depicted in Figure 2(b). From this figure we observe that the fluid velocity diminishes for enhancing the values of ϕ . The influence of the concentration Grashof number G_n on velocity is shown in Figure 2(c). Since the concentration Grashof number G_n is the ratio of buoyant forces to viscous forces, it has an inverse relationship with viscosity. Because high viscosity restricts blood flow, and low viscosity increases blood flow velocity through the human body, the end result is high blood pressure. As a result, bigger quantities of concentration Grashof number G_n are required to slow blood flow.

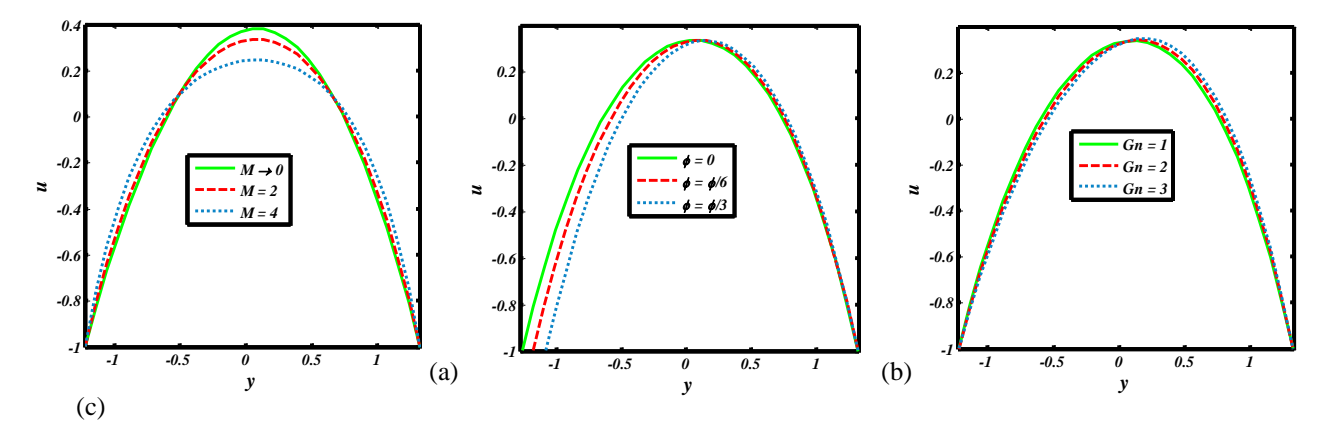


Figure 2.Variation of velocity for (a) M , (b) $\, \varphi \,$ and G_n with $\, \Theta = 1.9, d = 1.1, a = 0.4,$

$$M = 2, G_t = 0.5, b = 0.3, \phi = \frac{\pi}{6}, \varpi = 0.1, N_t = 0.2, N_b = 0.3, x = 0.1, p = 1$$

We examine the changes in velocity distribution as the Grashof number G_n increases from lower to higher levels. Because the acceleration in Grashof number G_n increased buoyant forces while decreasing viscous forces, the velocity profile improved. The axial velocity is observed to decrease in the region y > 0.1, however after the centerline, the velocity behavior reverses and becomes dominant in the region y > 0.1.

ISSN: 1001-4055 Vol. 44 No.6 (2023)

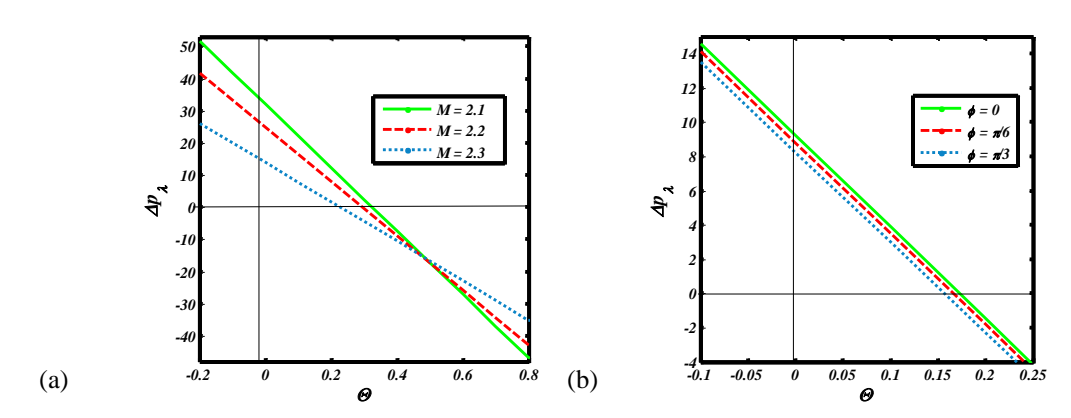


Figure 3. Variation of Pressure rise for (a) M and (b) ϕ with $M=2,G_t=0.5,G_n=0.5,b=0.3,$

$$\phi = \frac{\pi}{6}, \varpi = 0.1, N_t = 0.2, N_b = 0.3, x = 0.1, p = 1$$

At the midline y=0.1,, all of the graphs blend, indicating that this is the intermediate region of the velocity profile and that all fluid particles have the same velocity at this point. However, the extreme flows occur at the peristaltic wall's right and left ends. Figure 3(a) and (b) plotted for variation of pressure rise for Hartmann number and phase difference against Θ . From Figure 3(a), it reveals that, the pressure rise of Al_2O_3/H_2O nanofluid is lowered in the retrograde region ($\Delta p>0,\Theta<0$), peristaltic pumping region ($\Theta>0,\Delta p>0$). Pressure rise diminishes in the augmented pumping regions ($0\leq\Theta\leq0.5$) and boosts in ($\Theta>0.5$). As seen in Figure 3(b), the pressure rise decreases everywhere the phase angle values are improved.

4.2. Temperature and concentration

There are numerous uses for biomedical engineering that rely on mass and bioheat transfer via peristaltic motion. Thermal energy exchanges between various physical system components are related to the process of heat transfer. Heat transfer rate is generally dictated by the physical characteristics of a medium and the temperature difference between compartments. Bouyancy force affects a fluid's movement through a medium, whether it is Newtonian or not. The movement of fluid transports heat from one spot to another and from one particle to another during convective heat transfer. Furthermore, heat transport includes tissue conduction, heat convection caused by blood flow through pores in tissues, and hemodialysis, vasodilation, and oxygenation.

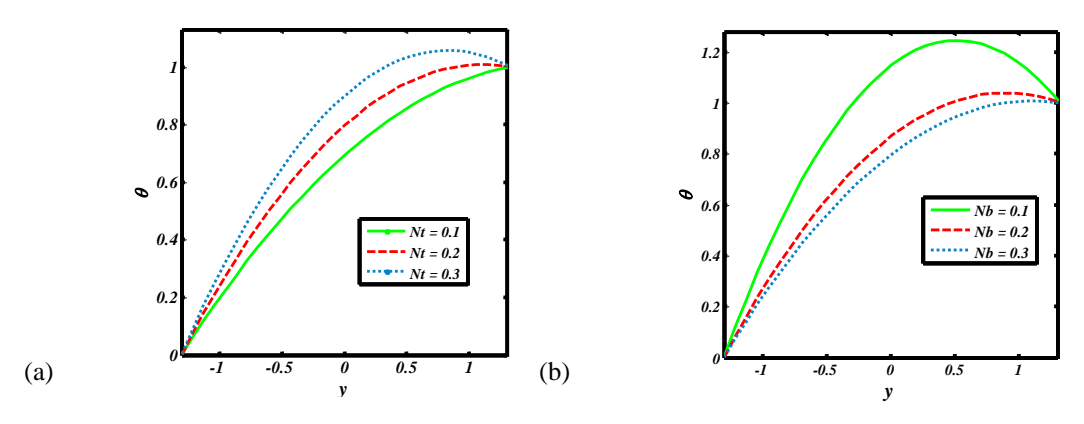


Figure 4. Variation of Temperature for (a) N_t and (b) N_b with $b = 0.5, \Theta = 1.9, d = 1.1, <math>\phi = \frac{\pi}{6}, x = 0.1,$ $\varpi = 0.1, a = 0.4, N_t = 0.2, t = 0.1, p = 1.$

The temperature profile for the thermophoresis parameter Nt is shown in Figure 4(a). The values of Nt clearly characterize the intensity of thermophoretic effects. Increasing the thermophoresis parameter Nt values improves the temperature profile. Physically, the thermophoresis parameter Nt increases the density of the thermal boundary layer, resulting in an increase in temperature as thermophoresis increases. For greater Nt values, boundary layer thickness is greater. In thermophoresis, tiny particles are pushed from a warm surface to a cold one, thereby increasing the temperature. Brownian diffusion coefficient Nb versus temperature profile are depicted in Figure 4(b). With an increase in Nb, the temperature profile in the channel falls. Figure 5(a) depicts the concentration profiles for various values of Nt. The concentration in the channel falls with increasing Nt. The effect of Nb is illustrated in Figure 5(b). This graph demonstrates that the concentration increases as the

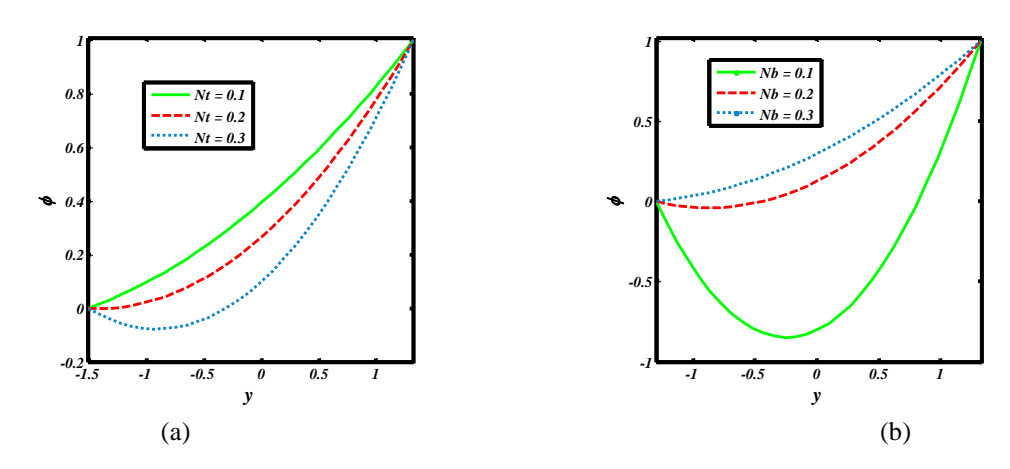


Figure 5. Variation of Concentration for (a) N_{t} and (b) N_{b} with

$$b = 0.5, \Theta = 1.9, d = 1.1, \phi = \frac{\pi}{6}, x = 0.1, \varpi = 0.1, a = 0.4, N_t = 0.2, t = 0.1, p = 1$$

4.3. Trapping phenomenon

Brownian coefficient Nb increases.

The process of streamlines capture is one of the most important peristaltic pumping phenomena. In essence, closed streamlines generate a fluid bolus that circulates organically. This bolus was captured and propelled forward by peristaltic movement.

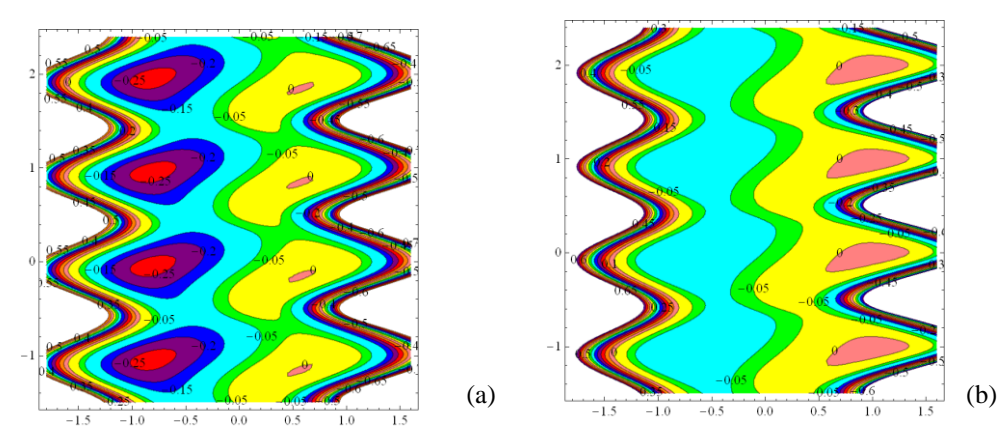


Figure 6. Streamlines for (a) M=1 and (b) M=4 with $b=0.3, G_n=0.5, G_t=0.5$,

$$\Theta = 1.9, d = 1.1, a = 0.4, \phi = \frac{\pi}{6}, \varpi = 0.1, N_t = 0.2, N_b = 0.3, x = 0.1.$$

Figures 6(a,b) show the behavior of streamlines in relation to the Hartmann number. The size of the trapped bolus diminishes in the left wall and enhances in the right wall when the magnetic M parameter is increased. In addition, the trapped bolus disappear in the left wall for larger magnetic parameter M. The phase difference on the streamlines changes, as seen in Figures 7(a,b). The middle region's emerging bolus is observed to move leftward and get smaller as it gets better. The bolus disappears and the streamlines travel parallel to the boundary walls at greater phase differences.

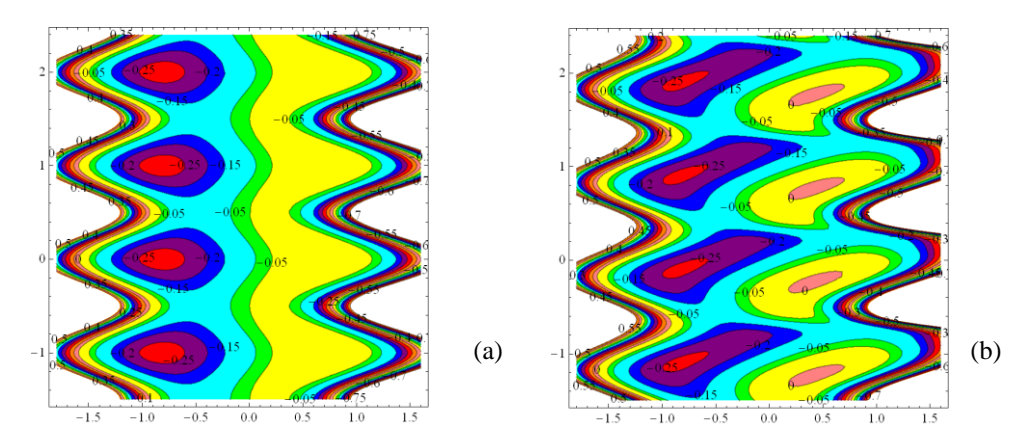


Figure 7. Streamlines for (a) $\phi \rightarrow 0$ (b) $\phi = \frac{\pi}{3}$ with $M = 1, b = 0.3, G_n = 0.5, G_t = 0.5,$

$$\Theta = 1.9, d = 1.1, a = 0.4, \ \phi = \frac{\pi}{6}, \varpi = 0.1, N_t = 0.2, N_b = 0.3, x = 0.1$$

5. Conclusion

In this paper, we studied heat and mass transfer analysis on the effect of magnetic field of (Al_2O_3/H_2O) nanofluid through vertical asymmetrical channel under the peristalsis. Key findings of impact of various flow parameters are presented below.

- \triangleright Velocity of the fluid reduces for M enhances.
- Pressure rise diminishes in the retrograde and peristaltic region when M enhances but rises in the augmented pumping region. Pressure lowered throughout the region when ϕ rises.
- Nanofluid temperature enhances for larger Thermoporesis parameter but opposite trend concluded in the concentration profile.
- > Temperature and nanofluid volume fraction diminishes for Brownian motion parameter boosts.

References

- [1] Shapiro A H, Jaffrin M Y and Weinberg S L 1969 J. Fluid Mech. 37 799–825.
- [2] Magesh A, Kothandapani M and Pushparaj V 2021 J. Phys.: Conf. Ser. 1850:012102
- [3] Magesh A, Praveen Kumar P, Tamizharasi P, Vijayaragavan R, Vimal Kumar S and KothandapaniM 2021 *J. Phys.: Conf. Ser.* **1850** 012111.
- [4] Bhatti M M, Zeeshan A, Ellahi R, Bég O A and Kadire A 2019 Chin J Phys 58:222–234.
- [5] Vijayaragavan R, Tamizharasi P and Magesh A 2022 J. Porous Media 25(6):65-81.
- [6] Kamalakkannan J, Dhanapal C, Kothandapani M. and Magesh A 2023 *Indian J. Phys.* Doi.12648-023-02636-9.
- [7] Tamizharasi P, Vijayaragavan R and Magesh A 2021 Partial Diff. Eqn. Appl. Math. 4:100087.
- [8] Choi S U S 1995 ASME J. Heat Transf. 66:99–105.

TuijinJishu/Journal of Propulsion Technology

ISSN: 1001-4055 Vol. 44 No.6 (2023)

- [9] Abdelsalam S I and Bhatti M M 2018 RSC Adv. **8**:7904–7915.
- [10] Hatami M, Mosayebidorcheh S and Jing D 2018 J. Anal. 27 (3):913-929.
- [11] Magesh A and Kothandapani M 2022 J. Mech. Med. Biol. 2(1):2150068.
- [12] Magesh A, Tamizharasi P and Vijayaragavan R 2022 Heat Transf. 51(7):6563-6577.
- [13] Tamizharasi P,Vijayaragavan R and Magesh A 2023 Math. Meth. Appl. Sci 46(1):13540-13557.
- [14] Magesh A.Tamizharasi P and Kamalakkannan J 2023 *Numer. Heat Trans. Part A: Appl.*1-18, https://doi.org/10.1080/10407782.2023.2240507.